

# Magnetic-field-induced changes in superparamagnetic cluster dynamics in the martensitic phase of $\text{Ni}_{43}\text{Co}_7\text{Mn}_{40}\text{Sn}_{10}$

P. L. Kuhns, M. J. R. Hoch, S. Yuan, A. P. Reyes, V. Srivastava, R. D. James, and C. Leighton

Citation: *Appl. Phys. Lett.* **108**, 252403 (2016); doi: 10.1063/1.4954732

View online: <http://dx.doi.org/10.1063/1.4954732>

View Table of Contents: <http://aip.scitation.org/toc/apl/108/25>

Published by the [American Institute of Physics](#)

---

## Articles you may be interested in

[Suppression of the ferromagnetic order in the Heusler alloy  \$\text{Ni}\_{50}\text{Mn}\_{35}\text{In}\_{15}\$  by hydrostatic pressure](#)

*Applied Physics Letters* **108**, 261903 (2016); 10.1063/1.4954838

[Adiabatic magnetocaloric effect in  \$\text{Ni}\_{50}\text{Mn}\_{35}\text{In}\_{15}\$  ribbons](#)

*Applied Physics Letters* **109**, 212402 (2016); 10.1063/1.4968592

[Uniaxial-stress tuned large magnetic-shape-memory effect in Ni-Co-Mn-Sb Heusler alloys](#)

*Applied Physics Letters* **110**, 071901 (2017); 10.1063/1.4976212

[Giant elastocaloric effect and its irreversibility in \[001\]-oriented  \$\text{Ni}\_{45}\text{Mn}\_{36.5}\text{In}\_{13.5}\text{Co}\_5\$  meta-magnetic shape memory alloys](#)

*Applied Physics Letters* **110**, 021906 (2017); 10.1063/1.4973965

[Magnetostuctural coupling and magnetocaloric effect in Ni-Mn-Ga-Cu microwires](#)

*Applied Physics Letters* **108**, 052401 (2016); 10.1063/1.4941232

[Magnetostuctural transition and magnetocaloric effect in highly textured Ni-Mn-Sn alloy](#)

*Journal of Applied Physics* **119**, 165102 (2016); 10.1063/1.4947503

---



## 5 Electronic Measurement Pitfalls to Avoid

Get the whitepaper

## Magnetic-field-induced changes in superparamagnetic cluster dynamics in the martensitic phase of $\text{Ni}_{43}\text{Co}_7\text{Mn}_{40}\text{Sn}_{10}$

P. L. Kuhns,<sup>1</sup> M. J. R. Hoch,<sup>1,a)</sup> S. Yuan,<sup>1</sup> A. P. Reyes,<sup>1</sup> V. Srivastava,<sup>2</sup> R. D. James,<sup>2</sup> and C. Leighton<sup>3</sup>

<sup>1</sup>National High Magnetic Field Laboratory, Florida State University, Tallahassee, Florida 32310, USA

<sup>2</sup>Department of Aerospace Engineering and Mechanics, University of Minnesota, Minneapolis, Minnesota 55455, USA

<sup>3</sup>Department of Chemical Engineering and Materials Science, University of Minnesota, Minneapolis, Minnesota 55455, USA

(Received 2 May 2016; accepted 12 June 2016; published online 22 June 2016)

The off-stoichiometric Heusler alloys, such as  $\text{Ni}_{50}\text{Mn}_{25+y}\text{X}_{25-y}$  ( $X = \text{Sn, In, Ga, etc.}$ ), have been extensively investigated using a variety of experimental techniques to probe their interesting and potentially useful magnetic properties. Recent  $^{55}\text{Mn}$  nuclear magnetic resonance (NMR) experiments, carried out largely in zero field (ZF) and making use of the large internal hyperfine field at the nuclear sites, have demonstrated the power of this approach in determining the ground state magnetic characteristics of these materials. In particular, the results reveal that distinct nanoscale ferromagnetic and antiferromagnetic phases coexist. A key parameter used in interpreting the NMR data is the transverse relaxation time  $T_2$  which, *inter alia*, determines the NMR blocking temperature  $T_B^{\text{NMR}}$  of magnetic regions. The present experiments on a polycrystalline sample of a specific illustrative alloy,  $\text{Ni}_{43}\text{Co}_7\text{Mn}_{40}\text{Sn}_{10}$ , which has received considerable attention, show that the application of relatively small external fields, comparable to or greater than the local anisotropy field in the ferromagnetic cluster regions, produces dramatic changes in  $T_2$  and hence  $T_B^{\text{NMR}}$ . The experimental findings are discussed using an extended version of a recently proposed nanocluster model for superparamagnetic systems. It is demonstrated that the field and temperature induced changes in  $T_2$  provide a significant test of the model and lead to a notable advance in applying the NMR technique to the investigation of the magnetic properties of this type of alloy. *Published by AIP Publishing.*

[<http://dx.doi.org/10.1063/1.4954732>]

Off-stoichiometric Heusler alloys with composition  $\text{Ni}_{50}\text{Mn}_{25+y}\text{X}_{25-y}$  ( $X = \text{Sn, In, Sb, etc.}$ ) exhibit unusually interesting magnetic, thermal, and structural behaviors that make them attractive for device development. Considerable attention has therefore been paid to understanding their physical properties.<sup>1–14</sup> Recent investigations of the quaternary system  $\text{Ni}_{50-x}\text{Co}_x\text{Mn}_{40}\text{Sn}_{10}$  ( $5 \leq x \leq 8$ ) have revealed particularly promising features for applications.<sup>15–23</sup> Specifically, the  $\text{Ni}_{50-x}\text{Co}_x\text{Mn}_{40}\text{Sn}_{10}$  phase diagram shows that as the temperature is lowered, the representative  $x = 7$  alloy undergoes a transition from a paramagnetic to ferromagnetic (FM) austenite (A) phase at  $T_C \approx 430$  K, followed by a displacive transition to a martensitic (M) phase at  $T_M \approx 370$  K.<sup>23</sup> The martensitic phase transformation in this alloy is of special interest as it features unusually low thermal hysteresis and a large magnetization decrease (the M phase does not exhibit long-range FM order).<sup>23</sup> The discontinuity in the magnetization at  $T_M$  thus facilitates a quasi-reversible field-induced M-A phase change, which, together with the observed magnetocaloric effect, provides opportunities in activators, sensors, magnetic refrigerators, and thermal-to-electrical energy conversion devices.<sup>24</sup>

The unusual magnetic properties of  $\text{Ni}_{50-x}\text{Co}_x\text{Mn}_{40}\text{Sn}_{10}$  at low temperatures in the M phase, which include superparamagnetism (SP) and intrinsic exchange bias (EB) effects,

have attracted considerable interest.<sup>21–23</sup> We have recently shown that  $^{55}\text{Mn}$  nuclear magnetic resonance (NMR) (performed primarily in zero applied field) provides considerable information on the microscopic magnetic nature of these alloys, wherein competing interactions give rise to nanoscale magnetic phase separation into FM and antiferromagnetic (AF) clusters.<sup>25,26</sup> A key parameter in the cluster model used to interpret the NMR results is the transverse nuclear relaxation time  $T_2$ . In particular, it is the behavior of  $T_2$  that determines what we have termed the NMR SP blocking temperature  $T_B^{\text{NMR}}$ .<sup>25</sup> The NMR spectrometer recovery time for the detection of spin echo signals following large amplitude radio frequency (RF) pulses is  $\tau_m \sim 10\mu\text{s}$ . A particular magnetic cluster in a heterogeneous material therefore has  $T_2 < \tau_m$  above  $T = T_B^{\text{NMR}}$  and the NMR signals from the region can no longer be detected at these temperatures. The cluster is thus unblocked, on the NMR timescale, for  $T > T_B^{\text{NMR}}$ .

The present experiments on the representative alloy  $\text{Ni}_{43}\text{Co}_7\text{Mn}_{40}\text{Sn}_{10}$  examine changes in the NMR spin echo response, and in particular that of the important parameter  $T_2$ , which are produced by an applied field  $\mu_0 H$  comparable to, or greater than, the anisotropy field in the FM clusters found in this material. The NMR results are analyzed using an extension of the zero field cluster model for nanoscale phase separated alloys that is mentioned above.<sup>25,26</sup> It is shown that the extended model can account for the changes in  $T_2$  with

<sup>a)</sup>Author to whom correspondence should be addressed: hoch@magnet.fsu.edu

$\mu_0 H$  and also with temperature. The work provides an essential extension of the NMR approach to the investigation of the magnetic properties of Heusler alloys and other SP systems.

Polycrystalline samples of  $\text{Ni}_{43}\text{Co}_7\text{Mn}_{40}\text{Sn}_{10}$  were produced by arc melting high purity metals, followed by thermal annealing, as described previously.<sup>19,22,23</sup> The samples were characterized using x-ray diffraction, neutron scattering, spectroscopic, thermal, and magnetization techniques.<sup>19,22,23</sup> Zero field (ZF) and low applied magnetic field  $^{55}\text{Mn}$  NMR measurements were made with a spin echo spectrometer operating in the range 200 to 450 MHz by making use of the large hyperfine field  $\mu_0 H_{hf}$  (20–45 T) at  $^{55}\text{Mn}$  sites. The transverse relaxation time  $T_2$  is determined from the decay of the spin echo amplitude with pulse spacing. In general, the decay curves exhibit stretched exponential behavior, i.e.,  $\exp - (t/T_2)^\beta$ , with  $\beta < 1$ . This indicates a distribution of  $T_2$  values due to the inhomogeneous nature of the alloy. When setting pulse lengths, allowance was made for changes in the NMR enhancement factor  $\eta$ , which are produced by changes in either  $H$  or  $T$ . The enhancement factor is related to the anisotropy field,  $H_A$ , via  $\eta = H_{hf}/H_A$ .<sup>25</sup>

Figure 1(a) plots the measured frequency  $f$  at  $T = 1.6$  K for a particular  $^{55}\text{Mn}$  spectral peak F2, which occurs at  $f_0 = 435$  MHz in ZF, as a function of  $\mu_0 H$ . It has previously been shown that the distinct spectral peaks at 400 and

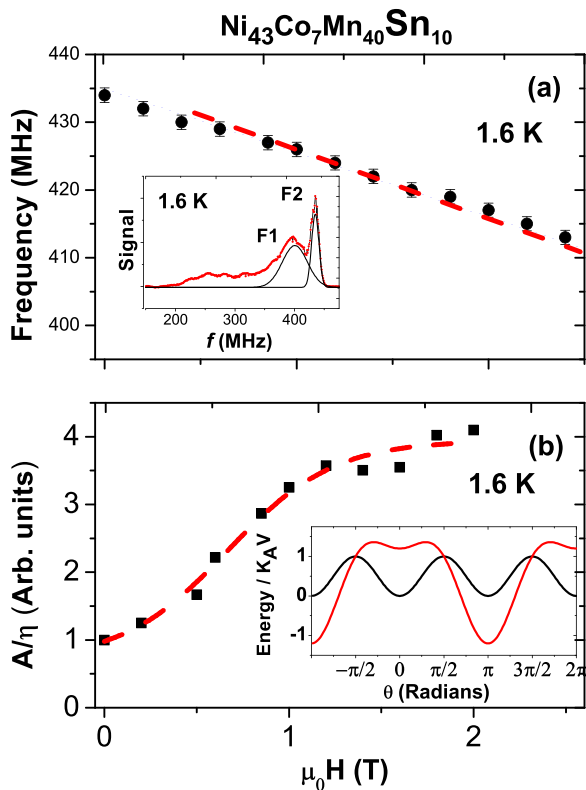


FIG. 1. Magnetic field dependence at 1.6 K of (a) the  $^{55}\text{Mn}$  resonance frequency for the component F2 of the NMR spectrum of polycrystalline  $\text{Ni}_{43}\text{Co}_7\text{Mn}_{40}\text{Sn}_{10}$ , which is shown in the inset and (b) the NMR signal amplitude of F2 after correction for changes in the signal enhancement factor  $\eta$  produced by the applied field. The slope of the dashed straight line through the data in (a) is given by  $-^{55}\gamma/2\pi = -10.5$  MHz while the sigmoidal fit in (b) is a guide to the eye. The inset in (b) gives the predicted form of the magnetic energy function in dimensionless units as a function of  $\theta$ , the angle the cluster spin makes with the easy axis. For convenience, the applied field is chosen parallel to the easy axis.

435 MHz, which are designated as F1 and F2 in the full ZF spectrum shown in inset to Fig. 1(a), are associated with Co rich FM clusters with  $T_B^{NMR} > 1.6$  K, as discussed in Ref. 26. (Note that we do not exclude the possibility that a fraction of smaller clusters remain unblocked on the NMR timescale even at 1.6 K.) Returning to Fig. 1(a) we expect  $f = f_0 - (\gamma/2\pi)\mu_0 H$  for the FM peaks, where  $\gamma/2\pi = 10.50$  MHz/T for  $^{55}\text{Mn}$ , and the slope of the dashed straight line in Fig. 1(a) for F2 is indeed  $-\gamma/2\pi$ . Similar results are obtained for F1. Fig. 1(b) shows the integrated area of peak F2 as a function of  $\mu_0 H$ . The areas were determined using multiple Gaussian spectral fits as given in the inset to Fig. 1(a). Allowance is made in Fig. 1(b) for changes in  $\eta$  (note the y-axis). A large part (factor  $\sim 3$ ) of the increase in the amplitude of F2 with  $\mu_0 H$  is due to field-induced alignment of cluster moments and hence  $H_{hf}$  at  $^{55}\text{Mn}$  sites. Optimal alignment occurs when nuclear spins are oriented parallel to  $H$  and perpendicular to the plane containing the transient RF field. A smaller contribution to the signal increase may be due to the in-field freezing of small volume SP clusters which in ZF are dynamic on the NMR timescale, with  $T_2 < 10$   $\mu\text{s}$ . At 1.6 K, the coercive field  $\mu_0 H_c$  is estimated at 0.3 T from magnetization measurements,<sup>22</sup> and Fig. 1(b) indeed shows that the amplitude of the NMR signal increases significantly for  $H > H_c$ .

We turn now to the behavior of  $1/T_2$  as a function of both  $\mu_0 H$  and  $T$ , which is central to this paper. Fig. 2 shows  $1/T_2$  vs.  $\mu_0 H$  in the range 0–2.5 T, while Fig. 3 is a log-log plot of  $1/T_2$  vs.  $T$  for  $\mu_0 H$  values of 0 and 1 T. From Fig. 2 it can be seen that for component F2 at 1.6 K the application of  $\mu_0 H = 1$  T leads to a decrease in  $1/T_2$  by a factor  $\sim 5$ . A similar decrease is found for component F1 (also shown). The inset in Fig. 2 gives the behavior with  $\mu_0 H$  of the stretched exponential exponent  $\beta$  for both F1 and F2. After an initial increase in the range  $0 \leq \mu_0 H \leq 0.5$  T,  $\beta$  reaches high field plateau values of 0.90 for F1 and 0.76 for F2.

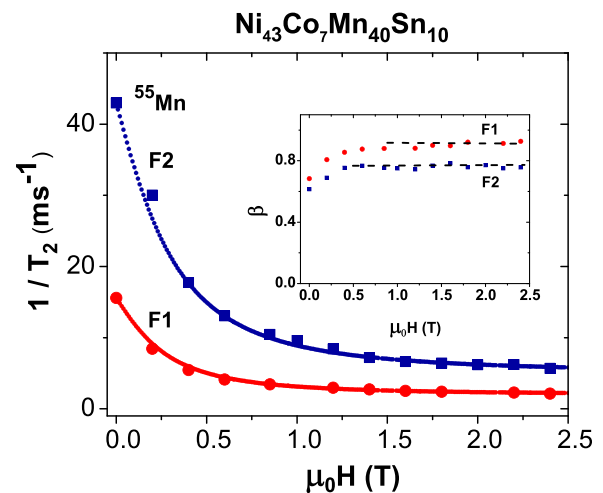


FIG. 2. Variation of the  $^{55}\text{Mn}$  spin-spin relaxation rate  $1/T_2$  in  $\text{Ni}_{43}\text{Co}_7\text{Mn}_{40}\text{Sn}_{10}$  as a function of applied field at 1.5 K for the F1 and F2 spectral components shown in the inset in Fig. 1(a). The curves shown are fits based on Eq. (2) and represent the cluster model predicted behavior with allowance for a competing relaxation mechanism in fields high compared to the anisotropy field. The inset gives a plot of the stretched exponential exponent  $\beta$  vs. field, showing plateau behavior above 0.5 T.

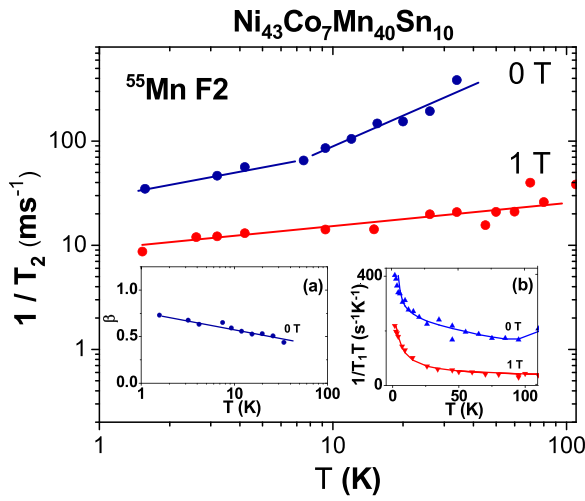


FIG. 3. Log-log plot of the  $^{55}\text{Mn}$  spin-spin relaxation rate  $1/T_2$  vs.  $T$  for  $\text{Ni}_{43}\text{Co}_7\text{Mn}_{40}\text{Sn}_{10}$ , measured in zero field and in 1 T, for the F2 spectral component specified in Fig. 1(a). The straight lines drawn through the data points are guides to the eye. The inset (a) shows a plot of the stretch exponent  $\beta$  vs.  $T$  in zero field. Inset (b) is a Korringa plot of  $1/T_1T$  vs.  $T$  based on spin-lattice relaxation rate data given in Ref. 26. The strong field dependence of  $1/T_1$  is attributed to field-induced changes in the inter-cluster dipolar interactions.

Figure 3 shows that for F2, the field-induced decrease in  $1/T_2$  persists to  $T > 35$  K, the highest temperature at which the ZF relaxation rate measurements were made. Similar behavior is found for component F1 (data not shown). The dashed straight lines through the points are guides to the eye. While spin echo signals were observed in ZF at temperatures above 35 K, the reduced signal-noise ratio prevents reliable measurements of  $T_2$  at higher  $T$ . For the  $\mu_0H = 1$  T case, the  $T_2$  measurements can be made above 35 K because of the field-induced increase in both the NMR signal amplitude (Fig. 1(b)) and  $T_2$ . Interestingly, the ZF  $1/T_2$  values show an abrupt change in  $T$  dependence around 7 K, as indicated by the significant difference in slope above and below 7 K. The inset (a) in Fig. 3 gives the behavior of the exponent  $\beta$  with  $T$  for component F2 in ZF. The steady decrease in  $\beta$  with increasing  $T$  points to a change in the relaxation rate distribution linked to thermally-induced changes in the cluster size distribution. Inset (b) in Fig. 3 is a Korringa plot of  $1/T_1T$  vs.  $T$  based on spin-lattice relaxation rate data given in Ref. 26. The strong field dependence of  $1/T_1T$  suggests that inter-cluster dipolar interactions, in addition to carrier scattering, are involved in the spin-lattice relaxation process. Dipolar interactions are likely to play a secondary role to intra-cluster dynamics in determining  $1/T_2$ . The low temperature collective intra-cluster oscillation mechanism, which is of central importance for  $1/T_2$  via nuclear spin dephasing, is unimportant for  $1/T_1$  which involves energy transfer to the lattice as discussed in Ref. 25.

In order to understand this in-field behavior of  $1/T_2$ , we first focus on the dynamical behavior of SP clusters in ZF, which is determined by the magnetocrystalline anisotropy energy  $E_A$  and involves the angle  $\theta$  between the cluster magnetization and the crystal easy axis. Assuming uniaxial magnetocrystalline anisotropy, this energy takes the form  $E_A = K_A V \sin^2\theta$ , displaying minima at  $\theta = 0$  and  $\pi$  (inset to

Fig. 1(b)).  $K_A$  here is the anisotropy energy density and  $V$  is the cluster volume.<sup>27,28</sup> For  $K_A V \gg k_B T$ , where  $k_B$  is Boltzmann's constant, we have  $\theta_m^2 = k_B T / K_A V$  with  $\theta_m^2$  the mean square amplitude of the collective spin oscillations. In general, both thermally activated intra-well and inter-well transitions between different energy states for a spin cluster need to be considered. The inter-well transition time  $\tau$  is given by the Néel-Arrhenius (NA) relation used, for example, in interpreting DC magnetization results for SP systems.<sup>22,25</sup>

Based on the SP dynamics model described above, we have previously obtained the following expression for the NMR transverse relaxation rate for a particular cluster of volume  $V$ <sup>25</sup>

$$\frac{1}{T_2} = \frac{1}{12} S(S+1) \left( \frac{\omega_I^2}{\omega_S^2} \right) \left( \frac{T}{T^*} \right)^2 \left( \frac{1}{\tau_c} \right). \quad (1)$$

Here,  $S$  is the Mn atom electron spin in the alloy,  $\omega_I = 2\pi f$ , with  $f$  the NMR frequency, and  $\omega_S = 2\pi/\tau_0$  involves the pre-exponential factor  $\tau_0$  used in the NA expression for SP clusters. For convenience, we define  $T^* = K_A V / k_B$ . For a system with a broad distribution of cluster sizes, there is a corresponding distribution of  $T^*$  values. The correlation time  $\tau_c$  is determined by the lifetime of a cluster in a particular energy state in a given potential well, i.e., it is associated with intra-well transitions, and is *not* the much longer inter-well characteristic time given by the NA expression. From an NMR perspective,  $\tau_c$  is the phase decoherence time for the fluctuating longitudinal hyperfine field at  $^{55}\text{Mn}$  sites.

It is useful to express the anisotropy field  $H_A$  in terms of  $K_A$  using  $K_A = \frac{1}{2} \mu_0 M H_A = \frac{1}{2} \mu_0 n \mu H_A$ , where  $M$ , the cluster magnetization, is given in terms of the spin density  $n$  in a cluster, with each spin having moment  $\mu$ . Application of a field comparable to or greater than  $H_A$  then leads to a change in the total magnetic energy given by  $E = E_A + E_H$ , with  $E_H = -\mu_0 \vec{M} \cdot \vec{H}$ , and hence to changes to the expression for  $1/T_2$ . For the special case in which the field  $H$  is applied *parallel* to the cluster easy axis, the cluster energy is given by  $E/K_A V = (\sin^2\theta \pm 2H/H_A \cos\theta)$ . Normalized illustrative plots of  $E/K_A V$  vs.  $\theta$  are shown in the inset in Fig. 1(b) for  $H = 0$  and  $H = 0.6H_A$ . As can be seen in the figure, a relatively small  $\mu_0 H$  produces a marked change in  $E$ .

In order to further quantify this discussion of field dependence, we now examine the behavior of  $T_2$  as a function of  $\mu_0 H$  for two different cases, as explained in detail below. For a particular cluster, with  $H$  at an angle  $\phi$  to  $H_A$ , the use of the cosine formula gives the effective anisotropy field as  $H_A^E = (H_A^2 + H^2 \pm 2H_A H \cos\phi)^{1/2}$  with the  $+$  ( $-$ ) sign corresponding to  $0 \leq \phi \leq \pi/2$  ( $\pi/2 \leq \phi \leq \pi$ ). For a polycrystalline sample in which the  $H_A$  are distributed over a sphere, it is necessary to evaluate hemispherical averages for  $H_A^E$  in each case. For the  $+$  case, in which  $H_A^E$  increases, we obtain  $\langle H_A^E \rangle = (H_A^2 + H^2 + H_A H)^{1/2}$ . Modifying the expression for  $T^*$  by replacing  $K_A$  by  $K_A^E$ , the field-dependence of  $1/T_2$  for a given cluster due to an applied field can be written as

$$\frac{1}{T_2(H)} = \frac{1}{T_2(0)} \left( 1 + \frac{H}{H_A} + \frac{H^2}{H_A^2} \right)^{-1}. \quad (2)$$

As an approximation, at a given  $T$  we neglect any changes in  $\tau_c$  produced by  $H$ . Equation (2) predicts that for clusters of a particular volume,  $1/T_2(H)$  should decrease steadily with  $H$  for  $H < H_A$  and then more rapidly for  $H > H_A$ . The alloy  $\text{Ni}_{43}\text{Co}_7\text{Mn}_{40}\text{Sn}_{10}$  has a distribution of F cluster sizes, however, which gives rise to a distribution of both longitudinal ( $1/T_1$ ) and transverse ( $1/T_2$ ) relaxation rates.<sup>26</sup> Additionally, the observed spin echo decay curves, from which  $T_2$  is determined, have stretched exponential form. For simplicity, we use the stretched exponential  $T_2$  values as an average over the cluster distribution. At a given temperature,  $1/T_2$  is largely determined by clusters with sizes in the vicinity of the most probable size and to a fair approximation the behavior will follow the predictions of Eq. (2). We therefore take  $T^* = \langle K_A V \rangle / k_B$ , where  $\langle K_A V \rangle$  represents an average of  $K_A V$  over the distribution.

If both  $T$  and  $H$  are allowed to vary, then with the use of Eq. (1), and again neglecting any changes in  $\tau_c$ , we obtain the following expression for clusters of a particular size:

$$\frac{1}{T_2(T, H)} \approx \frac{1}{T_2(T_0, H_0)} \left( \frac{T}{T^*(T, H)} \right)^2, \quad (3)$$

with  $T_0$  and  $H_0$  chosen as a reference temperature and a reference field, respectively. The behavior of  $T^*(T, H)$  with  $T$  and  $H$  depends on both  $K_A$  and  $V$ . In order to allow for a temperature-dependent distribution of  $V$  values, simulation of the stretched exponential spin echo decay curve, at given  $T$  and  $H$ , could be generated by numerical integration over a selected volume distribution (e.g., Gaussian) and the results used to predict, for example, the  $T$  dependence of  $1/T_2(T, H)$  at a particular  $H$ . In the interest of simplicity, however, we have simply used Eqs. (2) and (3) in the discussion of the results given below. We note that the use of Eq. (2) with fixed  $T$ , and correspondingly a stable cluster size distribution, is expected to provide a good approximation to the  $H$ -dependent observations, while the more general Eq. (3), which allows for changes in both  $T$  and  $H$ , is likely to be less reliable in accounting for the observed behavior since significant changes in the cluster size distribution may occur with increasing  $T$ .

The curves fit to the data in Fig. 2 are based on Eq. (2) with  $H_A$  as an adjustable parameter and with allowance for a small  $H$ -independent contribution, denoted by  $C$ , which is added to Eq. (2). This  $H$ -independent contribution becomes increasingly important for  $H > H_A$ . For F1, we find  $\mu_0 H_A = 0.35 \pm 0.05$  T and  $C = 2.0 \text{ ms}^{-1}$  while for F2, we get  $\mu_0 H_A = 0.4 \pm 0.05$  T and  $C = 5.0 \text{ ms}^{-1}$ . Encouragingly, the  $\mu_0 H_A$  values derived from the fits in Fig. 2 are fairly close to the 5 K coercive field  $\mu_0 H_C \approx 0.3$  T obtained for  $\text{Ni}_{44}\text{Co}_6\text{Mn}_{40}\text{Sn}_{10}$  from low-field magnetization hysteresis loops.<sup>22</sup> Previous independent estimates of  $\mu_0 H_A$  based on the ZF  $^{55}\text{Mn}$  NMR enhancement factor  $\eta$  in  $\text{Ni}_{43}\text{Co}_7\text{Mn}_{40}\text{Sn}_{10}$  at 1.6 K give  $\mu_0 H_A \approx 0.2$  T, with fairly large uncertainties ( $\sim 25\%$ ). The extracted  $\mu_0 H_A$  values are thus quite reasonable.

In order to understand the need for  $C$ , which captures the high  $H$  plateau in Fig. 2, it is necessary to consider other relaxation mechanisms involving, for example, inter-cluster dipolar interactions which become important in the long  $T_2$  limit. As noted above, evidence for the role of inter-cluster

dipolar interactions has previously been obtained from the field-dependence of the spin-lattice relaxation rate in  $\text{Ni}_{43}\text{Co}_7\text{Mn}_{40}\text{Sn}_{10}$  as shown in the Korringa plot (based on Ref. 26 results) given in inset (b) in Fig. 3. Furthermore, the plateau behavior of  $\beta$ , at comparatively high values as shown in the inset to Fig. 2 for  $\mu_0 H > 0.5$  T, is also an indicator of changes in the relaxation mechanism, from intra-cluster dynamics to an inter-cluster mechanism involving rapidly flipping small SP clusters.

The above results show that the intra-cluster dynamics model, used in the fit procedure for  $0 \leq \mu_0 H \leq 2H_A$  in Fig. 2, and which assumes an *averaged* spheroidal cluster size, provides a simple but useful basis for analyzing the NMR  $T_2$  data. The distribution of cluster sizes gives rise to an average  $T^*$  which involves  $\langle K_A V \rangle$  at a given  $T$ . We note for context that a spheroidal cluster of radius 2 nm has  $T^* \approx 200$  K in ZF, and the value of  $T^*$  increases rapidly as the cluster volume increases.

We turn now to the dependence of  $1/T_2$  on  $T$  for  $\text{Ni}_{43}\text{Co}_7\text{Mn}_{40}\text{Sn}_{10}$  in applied fields of 0 and 1 T as shown in the log-log plot in Fig. 3. As noted above, the ZF trend in  $1/T_2$  with  $T$  shows an abrupt change in slope around 7 K. The dashed straight lines, drawn as guides through the data points in Fig. 3, correspond to a  $T$ -dependence of the transverse relaxation rate given by  $1/T_2 \propto T^\nu$ . The exponent  $\nu$  changes from 0.4 to 1.0 for the ZF lines below and above 7 K, respectively. In contrast, for the 1 T case,  $\nu \sim 0.2$  and is constant over the range shown. We note that previous measurements on  $\text{Ni}_{43}\text{Co}_7\text{Mn}_{40}\text{Sn}_{10}$  have revealed that in ZF, the AF matrix, in which the FM clusters are embedded, becomes dynamic as  $T$  increases with  $T_B^{\text{NMR}} < 10$  K.<sup>26</sup> The above considerations suggest that it is the change in the dynamics of the AF clusters which causes the 7 K slope change at ZF in Fig. 3.

Finally, we note that the application of  $\mu_0 H = 1$  T results in the displacement of  $1/T_2$  to lower values than that in ZF at all  $T$ , as shown in Fig. 3. The  $\nu$  values obtained for the ZF and 1 T cases are different and significantly lower than the value  $\nu = 2$  inferred from Eq. (3). The fairly weak dependence of  $1/T_2$  on  $T$  implies that in the ratio  $T/T^*(T, H)$  in Eq. (3), an increase in  $T$  is offset, to some extent, by a change in  $T^*$ . Since  $T^* \propto \langle K_A^E V \rangle$ , Fig. 3 suggests that the cluster average  $\langle K_A^E V \rangle$  increases with  $T$  due to the unblocking of the low  $V$  clusters. Equation (3), with  $H$  constant, can be modified by taking  $T^* \propto T^\delta$  with  $\delta$  an exponent somewhat less than unity. The  $T$ -dependence of  $T^*$  reflects the decline in contributions to the NMR signal from the lower volume clusters in the distribution, as  $T$  exceeds their  $T_B^{\text{NMR}}$  values. These results demonstrate that the SP cluster model, with some allowance for a distribution of cluster volumes, provides a semi-quantitative method for analyzing the NMR relaxation rate results obtained for the F2 component in  $\text{Ni}_{43}\text{Co}_7\text{Mn}_{40}\text{Sn}_{10}$ , as a function of both  $\mu_0 H$  and  $T$ .

In summary, we have shown that the application of relatively small applied magnetic fields, comparable to the anisotropy field in nanoscale F clusters in the martensitic phase of the representative Heusler alloy  $\text{Ni}_{43}\text{Co}_7\text{Mn}_{40}\text{Sn}_{10}$ , produces significant changes in  $^{55}\text{Mn}$  NMR behavior and in particular in the transverse relaxation rate, which is of central importance in determining the spin echo response. The

findings are explained using a model in which the nanoscale cluster dynamics is altered by an applied field. Our analysis provides an instructive test of the cluster model. The model is applicable to other inhomogeneous magnetic systems in which nanoscale clusters are found and the approach can provide important information on the local magnetic properties.

The work at the National High Magnetic Field Laboratory was supported by NSF DMR-1157490 and by the State of Florida. Work at UMN in C.L.'s group was supported by DOE under Award No. DE-FG02-06ER46275. Work in R.D.J.'s group was supported by AFOSR-MURI (FA9550-12-1-0458), NSF-PIRE (OISE-0967140), and ONR (N00014-14-1-0714).

- <sup>1</sup>*Magnetism and Structure in Functional Materials*, edited by A. Planes, L. Mañosa, and A. Saxena (Springer, New York, 2005), Vol. 79.
- <sup>2</sup>T. Krenke, E. Duman, M. Acet, E. F. Wassermann, X. Moya, L. Mañosa, and A. Planes, *Nat. Mater.* **4**, 450 (2005).
- <sup>3</sup>T. Krenke, M. Acet, E. F. Wassermann, X. Moya, L. Manosa, and A. Planes, *Phys. Rev. B* **72**, 014412 (2005).
- <sup>4</sup>T. Krenke, M. Acet, E. F. Wassermann, X. Moya, L. Manosa, and A. Planes, *Phys. Rev. B* **73**, 174413 (2006).
- <sup>5</sup>G. D. Liu, X. F. Dai, S. Y. Yu, Z. Y. Zhu, J. L. Chen, G. H. Wu, H. Zhu, and J. Q. Xiao, *Phys. Rev. B* **74**, 054435 (2006).
- <sup>6</sup>P. J. Brown, A. P. Gandy, K. Ishida, R. Kainuma, T. Kanomata, K.-U. Neumann, K. Oikawa, B. Ouladdiaf, and K. R. A. Ziebeck, *J. Phys.: Condens. Matter* **18**, 2249 (2006).
- <sup>7</sup>P. J. Brown, T. Kanomata, K. U. Neumann, B. Ouladdiaf, A. Sheikh, and K. R. A. Ziebeck, *J. Phys. Condens. Matter* **22**, 506001 (2010).
- <sup>8</sup>M. Khan, I. Dubenko, S. Stadler, and N. Ali, *J. Phys. Condens. Matter* **20**, 235204 (2008).
- <sup>9</sup>S. Aksoy, M. Acet, P. P. Deen, L. Mañosa, and A. Planes, *Phys. Rev. B* **79**, 212401 (2009).
- <sup>10</sup>M. Ye, A. Kimura, Y. Miura, M. Shirai, Y. T. Cui, K. Shimada, H. Namatame, M. Taniguchi, S. Ueda, K. Kobayashi, R. Kainuma, T. Shishido, K. Fukushima, and T. Kanomata, *Phys. Rev. Lett.* **104**, 176401 (2010).

- <sup>11</sup>P. Entel, M. Stewart, M. E. Gruner, H. C. Herper, D. Comtesse, R. Arroyave, N. Singh, A. Talapatra, V. V. Sokolovsky, V. D. Buchelnikov, F. Albertini, I. Righi, and V. A. Cherenko, *Eur. Phys. J. B.* **86**, 65 (2013).
- <sup>12</sup>Z. Li, C. Jing, J. Chen, S. Yuan, S. Cao, and J. Zhang, *Appl. Phys. Lett.* **91**, 112505 (2007).
- <sup>13</sup>M. Khan, I. Dubenko, S. Stadler, and N. Ali, *Appl. Phys. Lett.* **91**, 072510 (2007).
- <sup>14</sup>B. M. Wang, Y. Liu, P. Ren, B. Xia, K. B. Ruan, J. B. Yi, J. Ding, X. G. Li, and L. Wang, *Phys. Rev. Lett.* **106**, 077203 (2011).
- <sup>15</sup>R. Kainuma, Y. Imano, W. Ito, Y. Sutou, H. Morito, S. Okamoto, O. Kitakami, K. Oikawa, A. Fujita, T. Kanomata, and K. Ishida, *Nature* **439**, 957 (2006).
- <sup>16</sup>R. Kainuma, Y. Imano, W. Ito, H. Morito, Y. Sutou, K. Oikawa, A. Fujita, T. Kanomata, K. Ishida, S. Okamoto, and O. Kitakami, *Appl. Phys. Lett.* **88**, 192513 (2006).
- <sup>17</sup>D. Y. Cong, S. Roth, J. Liu, Q. Luo, M. Pötschke, C. Hürrieh, and L. Schultz, *Appl. Phys. Lett.* **96**, 112504 (2010).
- <sup>18</sup>D. Y. Cong, S. Roth, M. Pötschke, C. Hürrieh, and L. Schultz, *Appl. Phys. Lett.* **97**, 021908 (2010).
- <sup>19</sup>V. Srivastava, X. Chen, and R. D. James, *Appl. Phys. Lett.* **97**, 014101 (2010).
- <sup>20</sup>W. Ito, X. Xu, R. Y. Umetsu, T. Kanomata, K. Ishida, and R. Kainuma, *Appl. Phys. Lett.* **97**, 242512 (2010).
- <sup>21</sup>D. Y. Cong, S. Roth, and L. Schultz, *Acta Mater.* **60**, 5335 (2012).
- <sup>22</sup>K. P. Bhatti, S. El-Khatib, V. Srivastava, R. D. James, and C. Leighton, *Phys. Rev. B* **85**, 134450 (2012).
- <sup>23</sup>K. P. Bhatti, V. Srivastava, D. P. Phelan, S. El-Khatib, R. D. James, and C. Leighton, in *Heusler Alloys*, edited by A. Hirohata and C. Felser (Springer, 2015).
- <sup>24</sup>Y. Song, K. P. Bhatti, V. Srivastava, C. Leighton, and R. D. James, *Energy Environ. Sci.* **6**, 1315 (2013).
- <sup>25</sup>S. Yuan, P. L. Kuhns, A. P. Reyes, J. S. Brooks, M. J. R. Hoch, V. Srivastava, R. D. James, S. El-Khatib, and C. Leighton, *Phys. Rev. B* **91**, 214421 (2015).
- <sup>26</sup>S. Yuan, P. L. Kuhns, A. P. Reyes, J. S. Brooks, M. J. R. Hoch, V. Srivastava, R. D. James, and C. Leighton, *Phys. Rev. B* **93**, 094425 (2016).
- <sup>27</sup>M. F. Hansen, C. B. Koch, and S. Mørup, *Phys. Rev. B* **62**, 1124 (2000).
- <sup>28</sup>L. T. Kuhn, K. Lefmann, R. H. Bahl, S. N. Ancona, P.-A. Lindgård, C. Frandsen, D. E. Madsen, and S. Mørup, *Phys. Rev. B* **74**, 184406 (2006).